DOI: 10.1002/cbic.200700524

Constrained Dansyl Derivatives Reveal Bacterial Specificity of Highly Conserved Thymidylate Synthases

Sanuele Calò,[a] Donatella Tondi,*[a] Stefania Ferrari,[a] Alberto Venturelli,[a] Stefano Ghelli,[b] and Maria Paola Costi*[a]

The elucidation of the structural/functional specificities of highly conserved enzymes remains a challenging area of investigation, and enzymes involved in cellular replication are important targets for functional studies and drug discovery. Thymidylate synthase (TS, ThyA) governs the synthesis of thymidylate for use in DNA synthesis. The present study focused on Lactobacillus casei *TS (LcTS) and* Escherichia coli *TS (EcTS), which exhibit 50% sequence identity and strong folding similarity. We have successfully designed and validated a chemical model in which linear, but not constrained, dansyl derivatives specifically complement the LcTS active site. Conversely, chemically constrained dansyl derivatives showed up to 1000-fold improved affinity for EcTS relative to the inhibitory activity of linear derivatives. This study demonstrates that the accurate design of small ligands can uncover functional features of highly conserved enzymes.*

Introduction

Thymidylate synthase (TS, ThyA; EC 2.1.1.45) is an essential enzyme for most living organisms. TS catalyzes the conversion of 2′-deoxyuridine-5′-monophosphate (dUMP) into 2′-deoxythymidine-5′-monophosphate (dTMP) by using N5,N10-methylenetetrahydrofolate (MTHF) as a cofactor. In most organisms, this pathway is the exclusive source of dTMP, which is essential for the synthesis of DNA. Recently, the mechanism of action of TS has been reconsidered.[1–3]

TS inhibition affects the DNA replication process and leads to thymineless death. Therefore, TS has been regarded as a target for anticancer drugs. The enzyme has also been implicated in the regulation of protein synthesis and in apoptotic processes, as well as in the development of Alzheimer's disease.[4] Recent interest in antibacterial agents that target TS has given rise to the challenging problem of finding species-specific inhibitors for highly conserved enzymes. In this context, *Lactobacillus casei* TS (LcTS) and *Escherichia coli* TS (EcTS) are the most frequently studied bacterial TSs.[5–6]

TS is an obligate homodimer with two active sites, each of which is formed by residues from both monomers. Comparative analysis of the known three-dimensional structures of TSs from different species shows that the overall protein fold is highly conserved; however, some structurally different domains are observed. The most variable regions are the small domain (SD) and the loop at the interface (HIL). LcTS is 316 amino acids long; the EcTS sequence is shorter, with 264 amino acids. The most variable region in LcTS and EcTS is the SD (residues 70–139 in the LcTS sequence, residues 68–87 in the EcTS sequence), which is 20 residues long in EcTS and 70 residues long in LcTS.[7,8]

Although the overall amino acid identity between LcTS and EcTS is only 50%, 39 of 55 residues within the substrate-binding domain, where substrates and classical inhibitors bind, are identical; therefore, it is difficult to discriminate between the two bacterial enzymes with known ligands. Classical TS inhibitors, such as folate-related compounds, bind tightly to the highly conserved folate binding site without discriminating between the two TS species.[9] However, nonclassical TS inhibitors that are structurally dissimilar from the substrate can discriminate specifically between the two bacterial species and are therefore important tools for probing species specificity for bacterial enzymes.[7,8,10–13]

By combining virtual screening with solid-phase in-parallel chemistry, a small library of *O*-dansyl-L-tyrosine derivatives was synthesized previously. Among these derivatives, *N*,*O*-didansyl-L-tyrosine (DDT) was the most potent inhibitor (K_i(LcTS) = 1.4 μM). Compounds **2L**–**9L** showed low-micromolar affinity for LcTS (Table 1).[10] DDT is a competitive inhibitor of TS versus the MTHF cofactor and is noncompetitive versus the substrate dUMP, which binds at a nearby site. DDT was selective for bacterial TS (LcTS and EcTS) over human TS.

Owing to the structural differences between the LcTS binding site and that of EcTS, we expected that a large molecule, such as DDT, would be unable to inhibit EcTS with the potency exhibited for LcTS. Surprisingly, DDT showed similar binding-affinity profiles for EcTS and LcTS (K_i(EcTS) = 1.8 μM, K_i(LcTS) = 1.4 μM). Therefore, a pronounced conformational rearrange-

[a] *Dr. S. Calò, Prof. D. Tondi, Dr. S. Ferrari, Dr. A. Venturelli, Prof. M. P. Costi*
Dipartimento di Scienze Farmaceutiche
Università degli Studi di Modena e Reggio Emilia
via Campi 183, 41100 Modena (Italy)
Fax: (+39) 059-205-5131
E-mail: donatella.tondi@unimore.it
mariapaola.costi@unimore.it

[b] *S. Ghelli*
SPINLAB s.r.l.
via Tamagno 3, 42048 Rubiera (RE) (Italy)

Supporting information for this article is available on the WWW under http://www.chembiochem.org or from the author.

Table 1. Activity of linear dansyl derivatives against LcTS and EcTS.

Code	Structure	K_i [μM] LcTS	EcTS
DDT	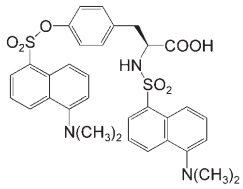	1.4	1.8
1L			
2L	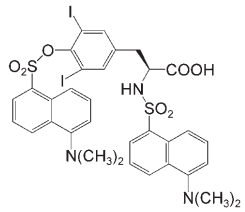	4.4	8.2
3L	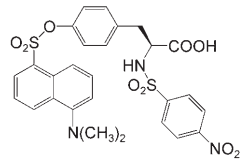	2.5	>1327[a] (*s*=75)
4L	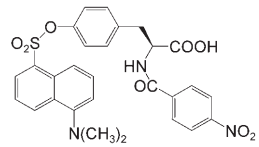	15	>1327[a] (*s*=72)
5L	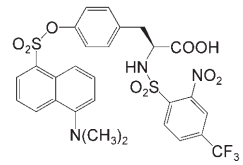	6.7	>636[a] (*s*=36)
6L	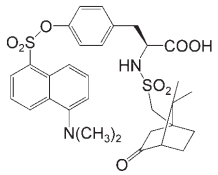	5.8	>1344[a] (*s*=76)
7L	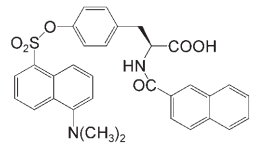	17	>1468[a] (*s*=83)
8L	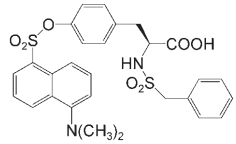	4.7	>1804[a] (*s*=102)
9L	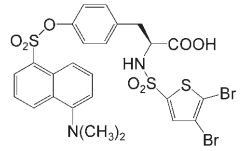	27	>1327 (*s*=75)

[a] Value calculated by assuming 2% inhibition at the solubility limit (*s* [μM]).

ment of DDT must occur to allow efficient binding to EcTS. X-ray crystallographic studies of EcTS and LcTS were carried out to investigate the binding orientation of DDT in each of the two active sites.

The X-ray crystal structure of DDT bound to EcTS provided evidence that DDT adopts a folded conformation in the EcTS binding site. The *O*-dansyl group (proximal dansyl ring) binds in the folate-binding domain at the same location as the quinazoline ring of the folate, and the *N*-dansyl group (distal dansyl ring) is folded over the tyrosine phenyl ring through stacking interactions (Figure 1 A).[10–14] Attempts to obtain the

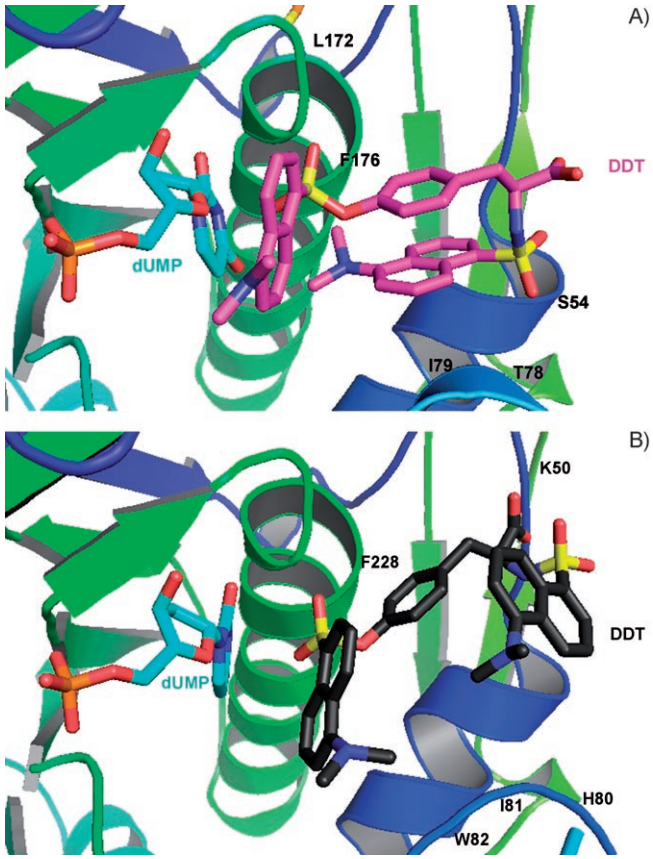

Figure 1. A) Details of the X-ray crystal structure of the ternary complex DDT–dUMP–EcTS: DDT bind to EcTS in a folded conformation. Protein structures are shown as ribbons. DDT and dUMP atoms are colored by atom type (C atoms of DDT in magenta and C atoms of dUMP in cyan). B) Predicted binding orientation of DDT in LcTS. DDT assumes a semifolded conformation. Protein structures are shown as ribbons. DDT and dUMP atoms are colored by atom type (C atoms of DDT in dark gray and C atoms of dUMP in cyan).

X-ray crystal structure of DDT bound to LcTS failed; however, molecular-dynamics studies on LcTS suggested that DDT could adopt two binding conformations: a folded and a semifolded conformation, whereby the latter is preferred (Figure 1 B).[6]

In a preliminary evaluation of the affinities of compounds **2L**–**9L** for EcTS, inhibitory activity was only detected for derivative **2L** (Table 1). These results suggest that compounds **3L**–**9L** can not assume a folded conformation that fits effectively into the active site. Chemical features of these molecules

might prevent them from adopting a folded conformation and thus preclude their binding to the EcTS enzyme. If this assumption is correct, a key code in discrimination between the two highly conserved TS enzymes could be revealed. To determine conclusively the contributions of linear and folded conformations of DDT and its derivatives toward the binding of these molecules to bacterial TSs, we designed and synthesized a series of constrained DDT analogues (Table 2).

The introduction of conformational constraints often modulates the chemical and biological properties of bioactive molecules and therefore serves as a useful chemical tool for investigating the conformational and structural requirements of enzyme–ligand interactions.[15–18] In the present case, a constrained DDT conformation could enhance entropically the binding affinity of DDT analogues for EcTS. The non-natural amino acid 1,2,3,4-tetrahydro-7-hydroxyisoquinoline-3-carboxylic acid (OH-Tic), a tyrosine derivative in which the side chain is part of a six-membered ring, was introduced into the structure of the dansylated molecule (Scheme 1) to provide local constraints in DDT derivatives.

Whereas converting the tyrosine functionality into a cyclic, rigid moiety contributes substantially to the immobilization of the final molecule, the α-amino group in the core serves as a derivatization point for the parallel introduction of different building blocks free to rotate along the N–SO_2 and the SO_2–R bonds. The building blocks introduced as substituents on the α-amino group were critical for exploring EcTS binding plasticity.

All **R** derivatives (rigid compounds) in the series were tested for their inhibitory activities against LcTS and EcTS, and their affinity profiles were compared with those of the **L** derivatives (linear analogues). The three-dimensional arrangements in solution of the rigid DDT analogue **1R** were investigated by high-resolution 2D NMR spectroscopy (COSY, HMQC, HMBC, and NOESY) to pinpoint a more stable conformation potentially related to the biological activity of **1R**.[19–20] Compound **1R** was then modeled in the EcTS binding site to elucidate its activity profile. The relationship between bacterial TS selectivity and the **1R** conformation elucidated from 2D NMR spectroscopy and modeling studies is discussed.

Results and Discussion

Design and synthesis

Previous results led us to conclude that dansyl derivatives do not have unique binding modes for the EcTS and LcTS active sites. Preliminary evaluation of the binding of compounds from set **L** to EcTS revealed that these linear compounds could not bind the enzyme efficiently (K_i = 0.6–1.8 mM). In contrast, the compounds from set **L** bind LcTS (K_i = 1.4–27 μM). Therefore, we decided to decrease the overall bulk of the molecules by using conformationally constrained analogues.

DDT is a highly flexible molecule in which two freely rotatable bonds connect the proximal dansyl group with the benzene ring, and five freely rotatable bonds connect the benzene ring with the distal dansyl group (Scheme 1). Folded and semifolded conformations have been described for the X-ray crystallographic structure of the EcTS–dUMP–DDT complex and the MD-modeled structure of the LcTS–dUMP–DDT complex (Figure 1A and B).[6,14] These conformations differ in the reciprocal positions of the tyrosine and distal dansyl rings. The folded conformation is characterized by an intramolecular π–π stacking interaction between the tyrosine and distal dansyl rings, which appear to be almost parallel to one another. In contrast, in the semifolded conformation, the intramolecular interaction between the tyrosine and distal dansyl rings has an edge-on orientation, with the aromatic rings located perpendicular to one another (Figure 1A and B).[21]

We designed and synthesized a series of structurally constrained DDT analogues (set **R**, Table 2) related to the linear derivatives described previously (set **L**, Table 1).[10] The conformationally constrained DDT derivatives were designed as rotationally locked analogues containing the constrained amino acid 1,2,3,4-tetrahydro-7-hydroxyisoquinoline-3-carboxylic acid (OH-Tic). The incorporation of this amino acid specifically restricts the rotation of the tyrosine side chain (Scheme 1) and was the primary synthetic modification to DDT and its derivatives. The secondary α-amino group was the derivatization point for the parallel introduction of different building blocks, in analogy with the synthesis of the linear dansyl derivatives (Table 1).

The N substituents introduced maintain significant conformational freedom along the sulfonamide/amide bond and, on the basis of the crystallographic structure of the DDT–EcTS complex, should explore additional subsites within the active

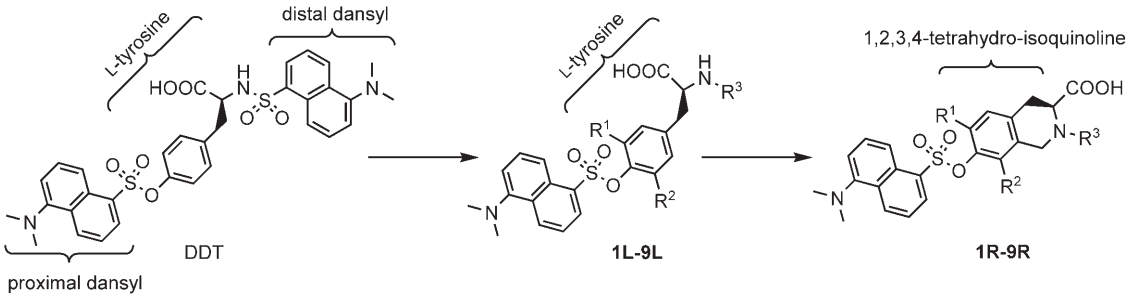

Scheme 1. Design of constrained DDT derivatives **1R**–**9R** related to *N,O*-didansyl-L-tyrosine (DDT, **1L**) and its derivatives **2L**–**9L**. The chemical constraint introduced in the tyrosine-derived portion of the molecule is highlighted.

Table 2. Activity of constrained dansyl derivatives against LcTS and EcTS.

Code	Structure	K_i [μM] LcTS	EcTS
rigid DDT **1R**	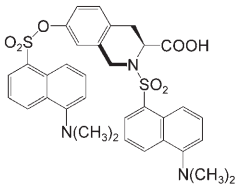	0.8	13
2R	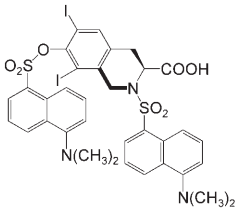	3.6	7.0
3R	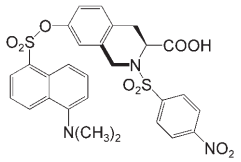	5.9	23
4R	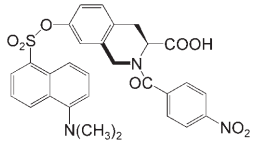	15	36
5R	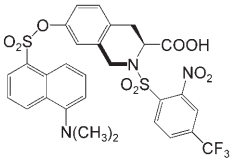	5.5	61
6R	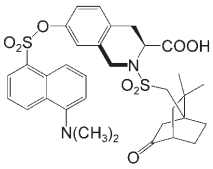	23	131
7R	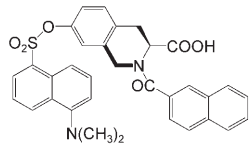	9.4	1529
8R	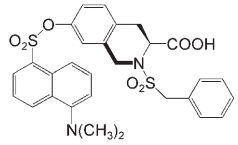	10	194
9R	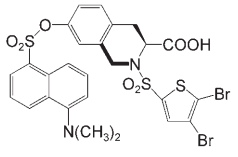	4	60

site of EcTS. In particular, four subsites delimit the entrance to the enzyme active site: T78, D81, E82, and W83 form the first subsite; H51, R53, S54, N76, T78, and the backbone of V77 form the second. The other two subsites are formed by K48, C50, H51, G257, K259, and the backbones of R49 and I258, and by K259, A260, and V262 (Figure 2).

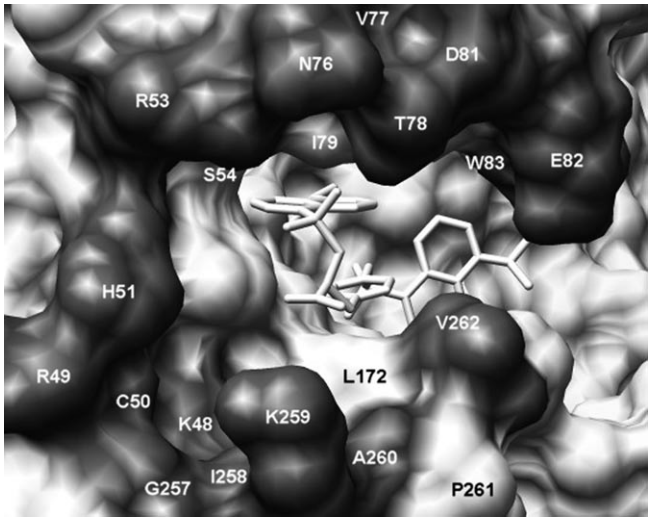

Figure 2. Four subsites form the entrance of the EcTS active site. T78, D81, E82, and W83 form the first subsite; H51, R53, S54, N76, T78, and the backbone of V77 form the second. The other two subsites are formed by K48, C50, H51, G257, K259, and the backbones of R49 and I258, and by K259, A260, and V262. Residues involved in key interactions with **1R** are labeled.

Compound **1R** has reduced flexibility, with three of the five freely rotatable bonds that connect the benzene ring with the second naphthalene ring in DDT frozen in the tetrahydroisoquinoline ring. This designed compound is a reasonable rigid model of the semifolded conformation observed for DDT bound to LcTS.

Constrained analogues of DDT were synthesized in five steps from the diiodo-substituted tyrosine derivative 3-(3,5-diiodo-4-hydroxyphenyl)-2-aminopropanoic acid (Scheme 2). Thus, a Pictet–Spengler reaction followed by the protection of the N atom with the acid-labile protecting group Boc gave **2A**. Next, catalytic dehalogenation provided the desired rigid core compound **4A** in high optical purity. Compound **4A** was treated with dansyl chloride, and the product **5A** was deprotected under acidic conditions to afford compound **6A**.[22] Compound **6A** was treated with the appropriate sulfonyl or acyl chlorides to afford compounds **3R**–**9R**. By alternative routes, product **1A** of the Pictet–Spengler reaction was converted into the rigid DDT analogue **1R** and the corresponding diiodo analogue **2R** (Scheme 2). Most products were isolated in good yields and underwent purification by crystallization (when indicated).

2D NMR spectroscopic determination of the conformation of 1R in solution

Compound **1R** was investigated by high-resolution 2D NMR spectroscopy (COSY, HMQC, HMBC, and NOESY) for the existence of a stable conformation in solution. In a preliminary experiment, DDT (**1L**) did not show any blocked conformations in solution at room temperature or −200 °C. In contrast, com-

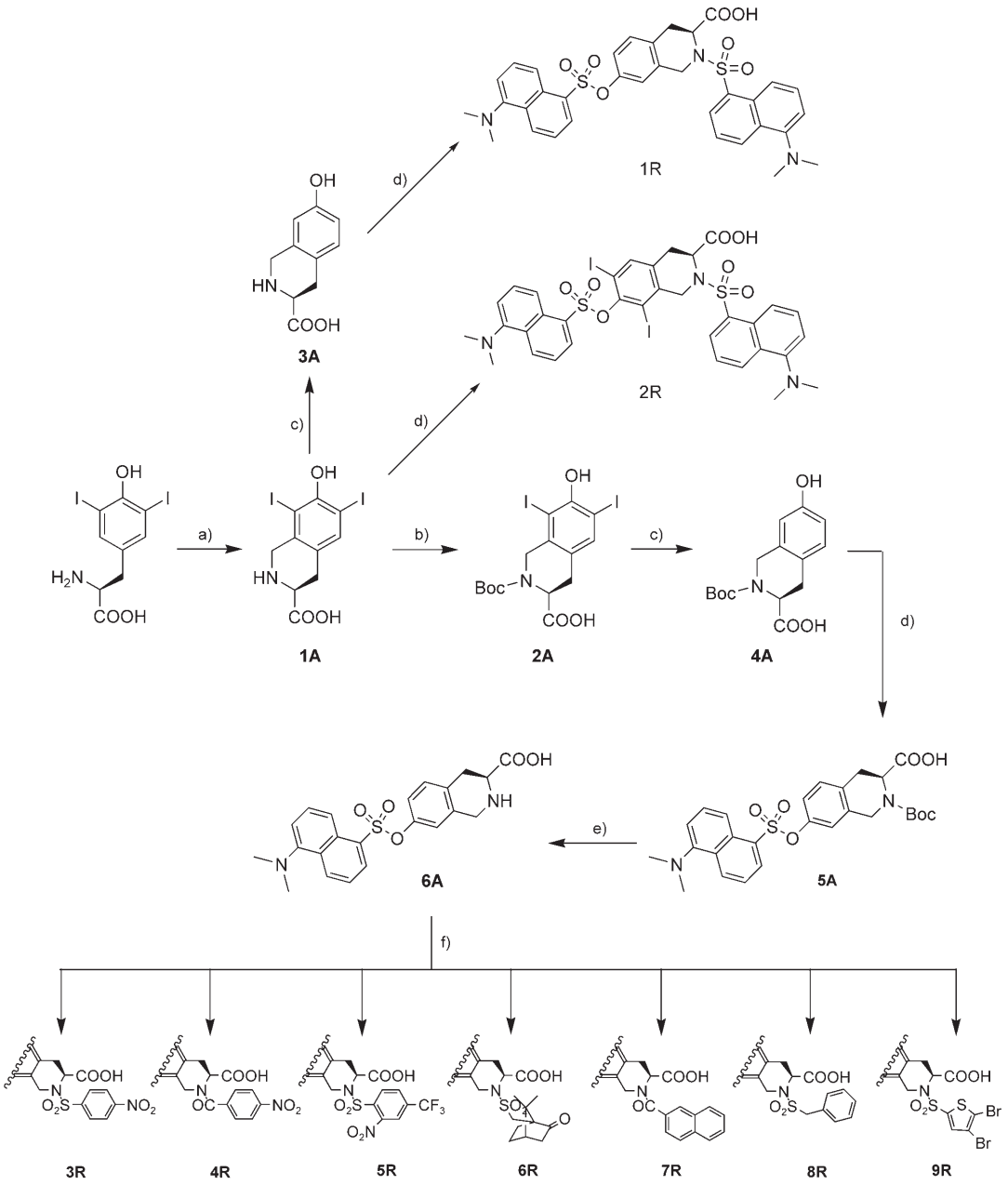

Scheme 2. Synthesis of constrained DDT analogues: a) CH_2O, $(CH_2OCH_3)_2$, HCl, 72–80 °C; b) Et_3N, DMF, H_2O, $(t\text{BuOCO})_2$, room temperature; c) Et_3N, MeOH, Pd/C, H_2, room temperature; d) dansyl chloride, $NaHCO_3$, NaOH, room temperature; e) CF_3COOH, CH_2Cl_2, room temperature; f) sulfonyl or acyl chloride, $NaHCO_3$, NaOH, room temperature. Boc = *tert*-butoxycarbonyl.

pound **1R** showed NOEs of interest at room temperature for the 1,2,3,4-tetrahydro-7-hydroxyisoquinoline-3-carboxylic acid moiety and the distal dansyl ring. The data obtained were used to determine the three-dimensional structure of rigid DDT (Figure 3A).

In all 2D NOESY spectra recorded at room temperature, the NOE between 10-H and 12-H_a, which has a coupling constant of 2.0 Hz with 13-H, is four times as strong as the NOE between 12-H_a and 12-H_b. The NOE between 12-H_b and 13-H is twice as intense as that observed between 12-H_a and 13-H (Figure 3A). Given the proportional dependence of NOE enhancement on $1/r^6$, these data suggest that in the three-dimensional model of rigid DDT, 12-H_a is closer to 10-H than to 12-H_b, and that 12-H_b is closer to 13-H than to 12-H_a (Figure 3A). NOEs of different intensities were observed for 14-H_a and 14-H_b of **1R**; in particular, 14-H_a ($\delta = 4.6$ ppm) is slightly farther than 14-H_b from 11-H ($NOE_{14\text{-}H_a\text{-}11}/NOE_{14\text{-}H_b\text{-}11} = 0.8$). However, in analogy with the results for DDT, no NOEs were observed for the proximal dansyl ring of **1R**, neither with the isoquinoline ring nor with the distal dansyl ring (Figure 3A). This result suggests that the proximal dansyl group has high conformational freedom.

Interestingly, the distal dansyl ring of **1R** seems to have lower conformational freedom than the proximal dansyl ring.

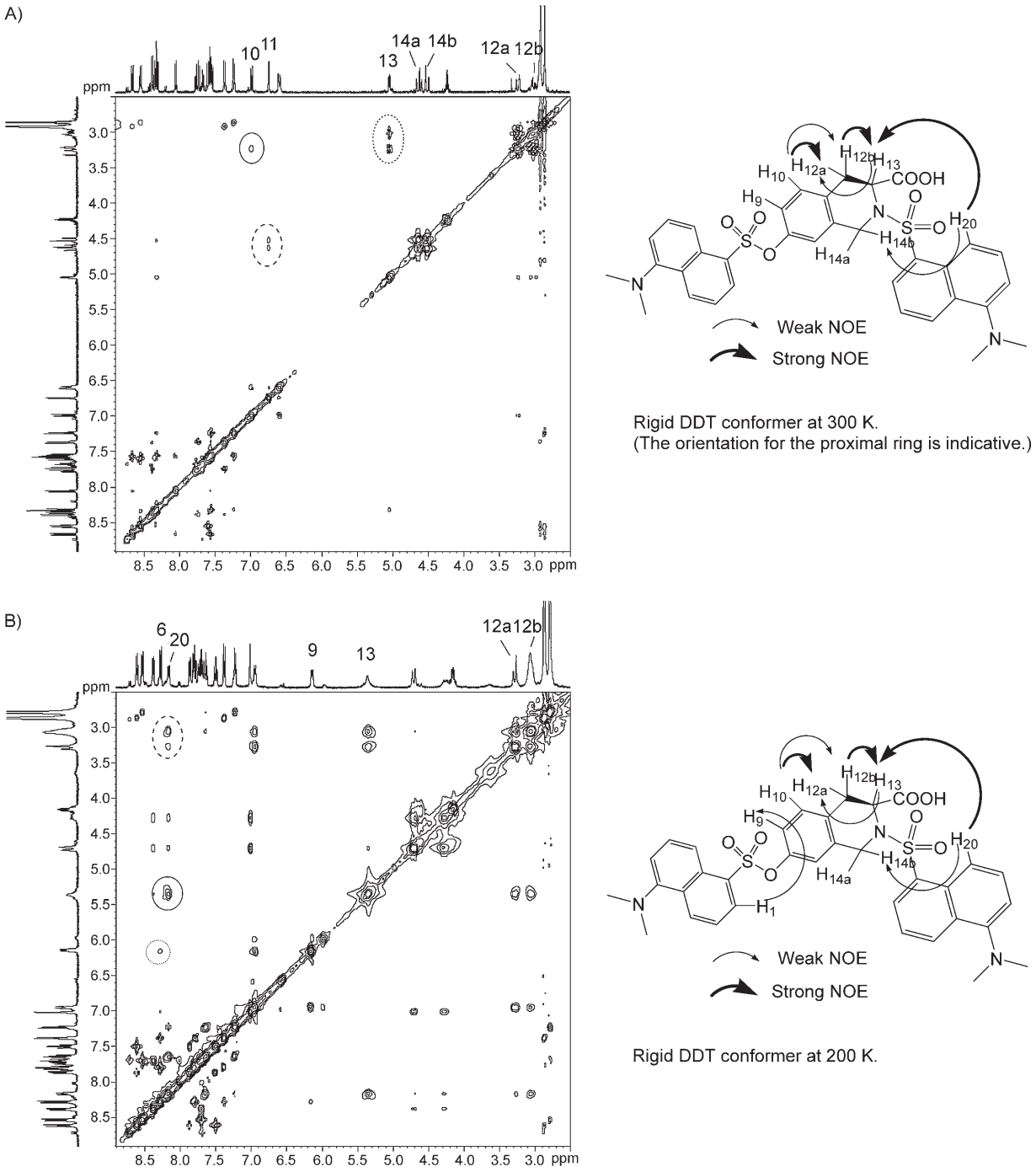

Figure 3. Determination of the conformation of **1R** by 2D NMR spectroscopy: NOESY experiment at A) 300 K and B) 200 K. Full ring: H10/H12a, dotted ring: H13/H12a and H13/H12b, dashed ring: H11/H14a and H11/H14b.

In the NOESY spectra, cross-peaks of different intensities between 20-H (distal ring) and 13-H, 14-H_a, and 14-H_b are present. The NOE between 20-H and 13-H is similar in intensity to that between 12-H_a and 10-H, whereas the NOE between 14-H_a and 20-H is 2.5 times weaker. The ratio $NOE_{14\text{-}H_a\text{-}20\text{-}H}/NOE_{14\text{-}H_b\text{-}20\text{-}H}$ is 0.6. The conclusion that 20-H is closer to 14-H_b and 13-H than to 14-H_a provides information on the conformation of the distal ring in **1R** (Figure 3A).

The conformation of **1R** at room temperature is similar to the semifolded conformation described for DDT in the MD-modeled structure of the LcTS–dUMP–DDT complex.[6] The distal dansyl and tetrahydroisoquinoline rings are close to one another and almost perpendicular. No preferred conformation can be described for the proximal dansyl moiety, as no NOE signals were observed.

Further 2D NMR experiments were carried out at low temperature to favor the formation of the more stable conformer of **1R**. During the temperature-dependent evolution of the ^1H NMR spectra, the movement of the signals for 9-H (−0.6 ppm), 13-H (0.5 ppm), 11-H (0.4 ppm), and 14-H_b (−0.3 ppm) is evi-

dent. Interestingly, the signals for two hydrogen atoms on the dansyl rings, 1-H (proximal) and 20-H (distal), move as the temperature is decreased (see the Supporting Information). Although the proximal dansyl ring showed no NOE signals at room temperature, an interaction between 6-H (proximal dansyl ring) and 9-H (benzene ring of tyrosine) was observed at low temperature. The intensity of this cross-peak was 80 times lower than that of the cross-peak observed between 12-H_a and 10-H (estimated distance: 3.6 Å). Two NOEs were observed for the distal dansyl ring at low temperature, one of which (between 20-H and 13-H) was also observed at room temperature. An additional NOE was observed between 20-H and 12-H_b. Therefore, with respect to the conformation adopted at room temperature, at low temperature the distal dansyl group moves toward the benzene ring. By integrating all detected NOEs, we estimated the internuclear distances between hydrogen atoms for which NOEs were observed. The results allowed the elucidation of the 3D structure of **1R** at low temperature (Figure 3B).

Prediction of the binding conformation of 1R in EcTS by molecular modeling

The conformation of **1R** determined in solution by means of 2D NMR spectroscopy was fitted to the crystallographic binding site of EcTS.[14] The *O*-dansyl moiety and the aromatic ring of the tetrahydroisoquinoline fragment, for which no preferred conformations were detected by NMR spectroscopic analysis, were modeled according to the conformation adopted by DDT in the X-ray crystal structure of the ternary DDT–dUMP–EcTS complex. This rigid match revealed a bad contact between the dimethylamino moiety and the side chain of T78 (Figure 4A). Therefore, the complex was energy minimized by a molecular mechanics method. In the resulting complex, the *O*-dansyl moiety (proximal dansyl group) forms electrostatic interactions with dUMP and the side chains of D169 and W83. The *O*-dansyl moiety also interacts through van der Waals interactions with W83, L143, L172, G173, V262, A263, and dUMP. The tetrahydroisoquinoline moiety of the molecule forms van der Waals interactions with E82, L172, A260, P261, and V262; the carboxylic group forms an electrostatic interaction with the backbone of V262 (NH group). The *N*-dansyl moiety forms electrostatic interactions with the side chains of R53, S54, N76, and T78 and van der Waals interactions with T78, I79, and E82 (Figure 4B).

Major differences were observed with respect to DDT in the binding of the *N*-dansyl moiety (distal ring) and in the orientation of the carboxylic functionality. These differences are related to the constrained tetrahydroisoquinoline ring of **1R** versus the tyrosine moiety of DDT. Two hydrogen bonds with S54 and T78, and the aromatic stacking interactions of the *N*-dansyl and tyrosine moieties with I79 and L172, are features of the binding of DDT that are lost in the complex with **1R**.

Analysis of the predicted binding orientation of **1R** explains how the constrained DDT analogue maintains a relatively good binding affinity for EcTS (K_i(DDT) = 1.8 μM, K_i(**1R**) = 13 μM; Figure 4C). Although the binding of the *O*-dansyl portion of **1R** closely resembles DDT binding in the EcTS folate domain, with

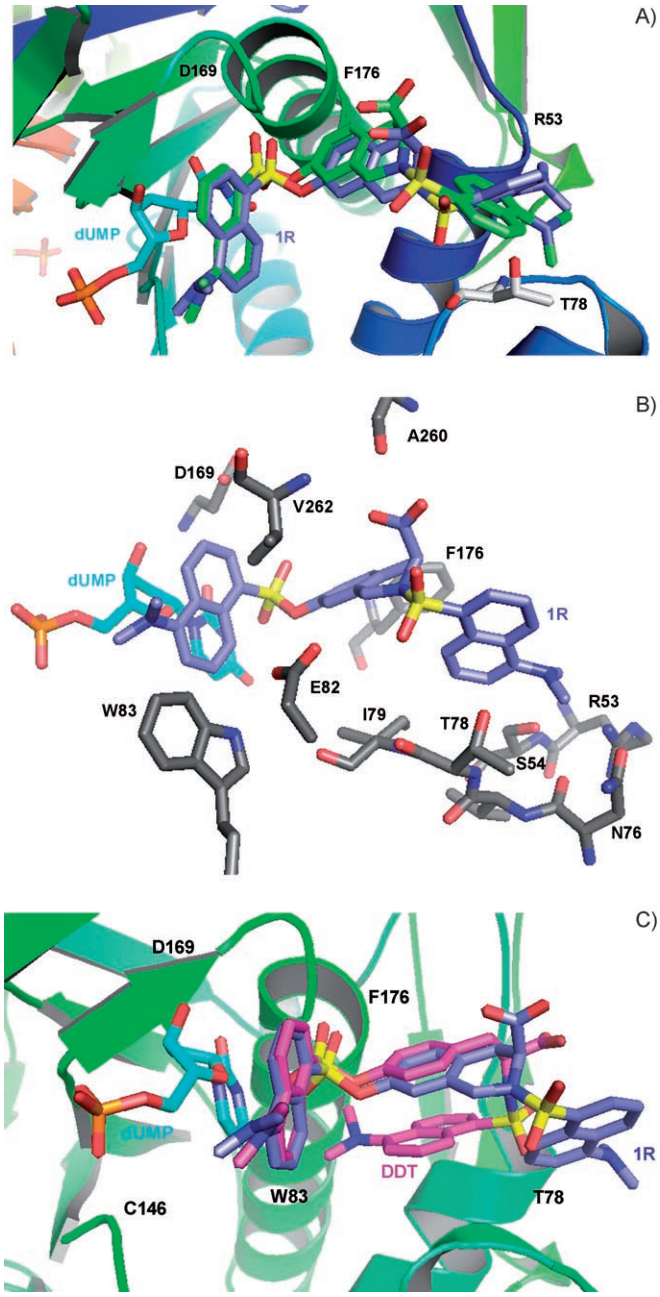

Figure 4. Conformation of **1R** as predicted by molecular modeling and as determined by NMR spectroscopy. A) Superimposition of the **1R** conformation determined by NMR spectroscopy (green) and the calculated **1R** conformation (blue). Unfavorable interactions exist between T78 and the nonminimized conformation determined by NMR spectroscopy. B) EcTS binding site of **1R**. Protein residues are colored by atom type, with C atoms in gray. Ligands are colored by atom type, with C atoms in blue. C) Superimposition of the EcTS–DDT–dUMP complex determined by X-ray crystallography and the predicted conformation of **1R**. Protein residues are shown as ribbons, and ligands are colored by atom type: C atoms of DDT in magenta for the X-ray crystal structure and in light blue for the predicted model.

1R a new electrostatic interaction is present between the carboxylic group and the backbone of V262 (NH group), as well as a dipole–quadrupole interaction between T78 and the *N*-dansyl moiety. The establishment of these new interactions between **1R** and EcTS probably minimizes the detrimental effect on binding of the constrained tetrahydroisoquinolinic moiety,

which causes the loss of the aromatic stacking interaction of the *N*-dansyl and tyrosine moieties with I79 and L172.

Comparison of the unbound conformation of **1R** as measured by NMR spectroscopy with the minimized/bound conformation of **1R** in the modeled ternary complex revealed several differences (Figure 4A). In particular, in the *N*-dansyl moiety, the torsions N–SO_2 and SO_2–R were rotated by approximately 40 and 60°, respectively. These conformational changes are necessary for the accommodation of the ligand in the active site of EcTS. In fact, without this rearrangement there would be a bad contact between the dimethylamino group of the *N*-dansyl moiety and T78. The heats of formation calculated from the AM1/SM2 Hamiltonian show that both conformations, bound and unbound, are favorable energetically (−203 and −177 kcal mol^{-1}, respectively); however, the bound conformation is more stable than the unbound conformation by approximately 26 kcal mol^{-1}.

Conformational analysis was performed on the N–SO_2 and SO_2–R torsions. The heats of formation of the 1296 conformers generated by increasing each torsion angle in increments of 10° indicate that these torsions are constrained (see the Supporting Information). Most energetically favorable conformations show that the SO_2–R torsion can rotate within the ranges 0–20, 60–155, and (−)110–0°, whereas the N–SO_2 torsion is constrained in the range 135–175°. There are two energetically equivalent optimal conformations: the first (conformer **1**) with N–SO_2 and SO_2–R torsion angles of 160 and 110°, respectively, and with a heat of formation of −204 kcal mol^{-1}, and the second (conformer **2**) with N–SO_2 and SO_2–R torsion angles of 150 and (−)40°, respectively, and with a heat of formation of −203 kcal mol^{-1}. Conformers **1** and **2** show very similar geometries to the conformations observed experimentally by low-temperature NMR spectroscopy (see the Supporting Information).

Molecular-modeling calculations of the stable conformers of compound **1R** reproduce nicely the geometries determined by NMR spectroscopy for the isolated molecule. When the conformer determined by NMR spectroscopy is fitted into the EcTS active site, an adaptation to the binding site is necessary to avoid bad contacts. The flexibilities of compound **1R** and the enzyme residues allow an energy-minimized complex to be formed.

Biological activity

All synthesized compounds were tested for binding to LcTS and EcTS (Table 1). The linear analogues **1L**–**9L** showed high to moderate affinities for LcTS (with K_i values that ranged from 1.4 to 27 μM). However, the linear compounds could not bind effectively to the EcTS enzyme, with the exception of 2′,6′-diiodo-DDT (**2L**), a close DDT analogue that shows an affinity profile similar to that of DDT (K_i = 1.8 and 8.2 μM for DDT and **2L**, respectively). Compounds **3L**–**9L** had lower affinities for EcTS by a factor of 10^2–10^3 ($K_i \gg$ 636-1804 μM). Thus, binding to EcTS appears to be governed by more-rigid structural requirements in terms of bulkiness and binding conformation than binding to LcTS (Table 1).

The correlation of structural changes with affinity for LcTS along the linear series revealed that the largest potency change occurred upon the conversion of a sulfonamide group into an amide (**3L** versus **4L**; DDT versus **7L**), a transformation which causes the activity to diminish by a factor of 6–12 (the K_i value increases from 1.4 to 17 μM for DDT, **3L**, **4L**, and **7L**).

The constrained derivatives **1R**–**9R** showed high to moderate affinities for LcTS (K_i = 0.8–23 μM; Table 2), as observed for the linear analogues. Rigidity was the discriminating aspect between the two series: Except for **7R**, the constrained derivatives showed good binding affinities for EcTS. These affinities were considerably improved with respect to those of the linear analogues; for example, **9R** was 20 times as active as the corresponding linear derivative toward EcTS. However, without exception, the rigid derivatives still bind more efficiently to LcTS than to EcTS (K_i = 7–194 μM).

The low affinity of **7R** for EcTS (K_i = 1529 μM) can be explained by steric hindrance caused by the naphthalene ring and the presence of an amide bond instead of a sulfonamide. The change in geometry from the nonplanar sulfonamide group to the planar carbamide functionality introduces additional rigidity in the fragment at the secondary α-amino group. Considering the overall reduced flexibility of the core structure of **7R**, the results obtained clearly indicate the critical effect of the *O*-dansyltetrahydroisoquinoline structure on the binding of the R fragmetns.

Structural inspection upon the binding of DDT derivatives accounts for a low level of specific binding interactions of the "distal" fragment. The K_i values for compounds **2R**–**6R** and **8R**–**9R** reflect a degeneration of the binding energies with increasing flexibility of the R fragment (see Scheme 1). This flexibility affects their ability to interact strongly with a specific region of the EcTS binding site. The structural determinant for the binding specificity is, as expected, the tetrahydrohydroxyisoquinoline core, which functions as an effective conformational constraint.

We conclude from the activity data that the active site of LcTS is better able to accommodate both linear and rigid molecules and is freer than the EcTS active site to rearrange conformationally. The latter active site has more restrictions in terms of recognition and binding interactions. Consequently, EcTS binds more tightly those molecules that can assume a folded/ordered binding mode, as observed for DDT in the EcTS crystal structure (folded conformation), or a semifolded conformation, as observed for **1R** in the 2D NMR spectroscopic studies.

Conclusions

The design of species-specific inhibitors able to discriminate between different highly conserved enzymes is a challenging problem. Species-specific discrimination is crucial for enzymes involved in cellular replication. TS is one of the best-known targets among these enzymes, as well as one of the most highly conserved enzymes. The high degree of conservation between LcTS and EcTS (up to 50% overall and greater than 70% between active sites) makes it difficult to identify ligands that can

discriminate between these enzymes. Previous studies revealed that a benzyloxycarbonylamino-*N*,*O*-didansyl-L-tyrosine derivative was able to discriminate between the two species, with a specificity index ($SI = K_i(EcTS)/K_i(LcTS)$) of 10^2.[10] Moreover, structural studies suggested the possibility of extending this finding to the entire family of dansyl derivatives.

To validate our chemical model, we synthesized **1R**, a dansyl derivative in which the isoquinoline moiety is a constrained analogue of the tyrosine residue in DDT, and introduced different substituents on the α-amino group. The new rigid compounds were able to bind EcTS, whereas the corresponding linear compounds could not. The SI of greater than 10^3 found in this case corresponds to an approximately tenfold increase with respect to that of the previously identified ligand. Thus, a key code for discriminating between the two highly conserved enzymes has been uncovered.

The low-energy conformation of the reference compound **1R** was determined by two-dimensional NMR spectroscopic studies, and molecular modeling studies demonstrated that the EcTS enzyme prefers to bind conformations in which the fragment attached to the constrained core is rotated by about 60°. These results reinforce the finding that EcTS can bind specifically only selected conformations. In conclusion, this study demonstrates that the accurate design of small ligands can reveal functional features of highly conserved enzymes.

Experimental Section

General: Dansyl-L-tyrosine, 3′,5′-diiodo-L-tyrosine, 3′-chloro-L-tyrosine, 3′-iodo-L-tyrosine, and sulfonyl chlorides were purchased from Aldrich, Sigma, and Fluka. The progress of reactions was monitored by TLC on silica-gel plates (Riedel-de-Haen, Art. 37341). Merck silica gel (Kieselgel 60, 230–400 mesh) was used for flash column chromatography. Elemental analyses were performed on a Perkin–Elmer 240C elemental analyzer; the results are within ±0.4% of the theoretical values. ^{1}H NMR and 2D NMR spectra were recorded on Bruker 200-MHz and 400-MHz spectrometers with tetramethylsilane as an internal standard. All chemicals used were of reagent grade. Yields refer to purified products and are not optimized.

3-(*S*)-1,2,3,4-Tetrahydro-7-hydroxy-6,8-diiodoisoquinoline-3-carboxylic acid (1A): (*S*)-2-amino-3-(3,5-diiodo-4-hydroxyphenyl)propionic acid (1.8 g, 3.8 mmol) was suspended in a solution of concentrated HCl (18 mL), 1,2-dimethoxyethane (1.2 mL), and formaldehyde (1.3 mL, 37% *w*/*w*). The white suspension was stirred and heated slowly to 72 °C over 30 min. Concentrated HCl (8 mL), 1,2-dimethoxyethane (0.6 mL), and formaldehyde (0.7 mL) were then added, and the mixture was stirred for 18 h at 72–75 °C. The suspension was then cooled, and the solid material was filtered off and recrystallized from MeOH/H_2O to give **1A** (41%). M.p. 220–225°; ^{1}H NMR ([D_6]DMSO, 200 MHz): $\delta = 7.72$ (s, 1-H), 4.03 (d, $J =$ 16.4 Hz, 4-H_a), 3.93 (d, $J = 16.4$ Hz, 4-H_b), 3.59 (dd, $J = 4.8$, 10.6 Hz, 3-H), 3.10 (dd, $J = 4.8$, 16.6 Hz, 2-H_a), 2.90 ppm (dd, $J = 10.6$, 16.6 Hz, 2-H_b); elemental analysis calcd (%) for $C_{10}H_9I_2NO_3$: C 26.99, H 2.04, N 3.15; found: C 26.79, H 2.22, N 3.26.

3-(*S*)-7-Hydroxy-6,8-diiodo-3,4-dihydro-1H-isoquinoline-2,3-dicarboxylic acid 2-tertbutyl ester (2A): Compound **1A** (1.62 g, 3.6 mmol) was dissolved in a mixture of Et_3N (0.1 mL), DMF (11.25 mL), and water (3 mL). Di-*tert*-butyldicarbonate (1.178 g, 5.4 mmol) was added, and the resulting mixture was stirred at room temperature for 5 h. The solvent was then removed, and the crude product was dissolved in 10% aqueous $KHSO_4$ (8 mL; pH 3–4) and extracted with EtOAc (3×20 mL). The organic phase was separated from the aqueous layer and dried over anhydrous Na_2SO_4, and the solvent was removed under reduced pressure. Recrystallization of the crude product from EtOAc/benzene afforded **2A** (83%). M.p. 160–165 °C; ^{1}H NMR ([D_6]DMSO, 200 MHz): $\delta = 7.72$ (s, 1-H), 4.85 (dd, $J = 2$, 6.8 Hz, 3-H), 4.57 (d, $J = 16.4$ Hz, 4-H_a), 4.29 (d, $J = 16.4$ Hz, 4-H_b), 3.20 (dd, $J = 2$, 6.8 Hz, 2-H_a), 3.14 (dd, $J = 6.8$, 16.4 Hz, 2-H_b), 1.53 ppm (s, 9H, Boc); elemental analysis calcd (%) for $C_{15}H_{17}I_2NO_5$: C 33.05, H 3.14, N 2.57; found: C 33.19, H 3.04, N 2.44.

3-(*S*)-1,2,3,4-Tetrahydro-7-hydroxy-isoquinoline-3-carboxylic acid (3A): Compound **1A** (3.46 g, 7.7 mmol) was dissolved in EtOH (12 mL), H_2O (5 mL), and Et_3N (0.6 mL), and the resulting mixture was hydrogenated at 203 kPa in the presence of Pd/C (10%) for 3 h with stirring. The catalyst was then eliminated by filtration, and the solution was acidified with dilute HCl to pH 6. The solid product was filtered and washed with cold H_2O to give **3A** (82%). ^{1}H NMR ([D_6]DMSO, 200 MHz): $\delta = 7.65$ (s, 1-H), 7.13 (d, $J = 8.2$ Hz, 2-H), 6.89 (d, $J = 8.2$ Hz, H-3), 3.5–4.6 (m, 2H, 6-$H_{a,b}$), 3.05 (t, $J = 5.0$, 10.4 Hz, 5-H), 2.95 (dd, $J = 5.0$, 17.4 Hz, 4-H_a), 2.80 ppm (dd, $J = 10.4$, 17.4 Hz, 4-H_a); elemental analysis calcd (%) for $C_{10}H_{11}NO_3$: C 62.17, H 5.74, N 7.25; found: C 62.33, H 5.64, N 7.13.

(*S*)-7-Hydroxy-3,4-dihydro-1*H*-isoquinoline-2,3-dicarboxylic acid 2-tertbutyl ester (4A): Compound **2A** (1.568 g, 2.9 mmol) was dissolved in MeOH (60 mL) and Et_3N (6 mmol), and Pd/C (10%; 0.186 g) was added to the solution. The mixture was stirred under H_2 pressure (2 atm) for 12 h at room temperature. The catalyst was then filtered off, and the filtrate was evaporated under vacuum. The product **4A** (71%) was obtained by using the same work up as for compound **2A**. M.p. 252–257 °C; ^{1}H NMR ([D_6]DMSO, 200 MHz): $\delta = 7.08$ (d, $J = 8.4$ Hz, 3-H), 6.69 (s, 1-H), 6.60 (d, $J =$ 8.4 Hz, 2-H), 4.92 (dd, $J = 2$, 6.8 Hz, 5-H), 3.28 (d, $J = 16.4$ Hz, 6-H_a), 3.10 (dd, $J = 2$, 16.4 Hz,4-H_a), 3.08 (d, $J = 16.4$ Hz, 6-H_b), 2.90 (dd, $J =$ 6.8, 16.4 Hz, 4-H_b), 1.53 ppm (s, 9H, Boc); elemental analysis calcd (%) for $C_{15}H_{19}NO_5$: C 61.42, H 6.53, N 4.78; found C 61.29, H 6.59, N 4.93

(*S*)-7-(5-Dimethylamino-naphthalene-1-sulfonyloxy)-3,4-dihydro-1*H*-isoquinoline-2,3-dicarboxylic acid 2-tert-butyl ester (5A): Compound **4A** (0.581 g, 1.98 mmol) was dissolved in aqueous 0.5 M $NaHCO_3$ (25 mL), and NaOH was added to pH 10. Dansyl sulfonyl chloride (1.5 equiv) was added at the reaction mixture, which was then stirred at room temperature overnight. The solution was then acidified to pH 4 with dilute HCl and extracted with EtOAc (3×20 mL). The organic phase was separated from the acqueous layer and dried over anhydrous $MgSO_4$, and the solvent was removed under reduced pressure. Recrystallization of the crude product from MeOH/H_2O afforded compound **5A** (77%) as a white solid. M.p. 125–130 °C; ^{1}H NMR ([D_6]DMSO, 200 MHz): $\delta = 8.71$ (d, $J = 8.6$ Hz, 3-H), 8.37 (d, $J = 8.6$ Hz, 6-H), 8.20 (d, $J = 7.8$ Hz, 1-H), 7.87 (t, $J = 8.4$ Hz, 5-H), 7.71 (t, $J = 8.4$ Hz, 2-H), 7.45 (d, $J = 8.6$ Hz, 4-H), 7.21 (d, $J = 8.2$ Hz, 10-H), 6.97 (s, $J = 2.2$ Hz, 11-H), 6.70 (d, $J =$ 8.2 Hz, 9-H), 4.91 (dd, $J = 2$, 6.8 Hz, 13-H), 4.50 (d, $J = 16.4$ Hz, 14-H_a), 4.40 (d, $J = 16.4$ Hz, 14-H_b), 3.01–3.26 (m, 2H, 12-$H_{a,b}$), 2.90 (s, 6H, 7-H, 8-H), 1.50 ppm (s, 9H, Boc); elemental analysis calcd (%) for $C_{27}H_{30}N_2O_7S$: C 61.58, H 5.74, N 5.32; found: C 61.45, H 5.87, N 5.25.

(*S*)-7-(5-Dimethylamino-naphthalene-1-sulfonyloxy)-1,2,3,4-tetrahydro-isoquinoline-3-carboxylic acid (6A): Trifluoroacetic acid

(1.3 mL) was added to a solution of **5A** (0.777 g, 1.48 mmol) in CH_2Cl_2 (3.9 mL), and the resulting mixture was stirred for 1 h at room temperature. The solvent was then removed under vacuum, and the crude product was washed several times with CH_2Cl_2 until no trifluoroacetic acid was detected. Recrystallization from water gave **6A** 82%). M.p. 190–195 °C; ^{1}H NMR ([D$_6$]DMSO, 200 MHz): δ = 8.74 (d, J = 8.6 Hz, 3-H), 8.38 (d, J = 8.8 Hz, 6-H), 8.21 (d, J = 7.6 Hz, 1-H), 7.89 (t, J = 7.8, 8.6 Hz, 5-H), 7.75 (t, J = 7.6, 8.4 Hz, 2-H), 7.48 (d, J = 7.6 Hz, 4-H), 7.29 (d, J = 8.4 Hz, 10-H), 7.18 (d, J = 2.4 Hz, 11-H), 6.76 (dd, J = 2.4, 8.2 Hz, 9-H), 4.40 (s, 2H, 14-H$_{a,b}$), 3.50 (dd, J = 5.5, 10.6 Hz, 13-H), 3.18 (dd, J = 5.5, 17.6 Hz, 12-H$_a$), 2.96 (s, 6H, 7-H, 8-H), 2.92 ppm (dd, J = 10.6, 17.6 Hz, 12-H$_b$); elemental analysis calcd (%) for $C_{22}H_{22}N_2O_5S$: C 61.96, H 5.20, N 6.57; found: C 62.14, H 5.10, N 6.49.

3-(*S*)-2-(5-Dimethylamino-naphthalene-1-sulfonyl)-7-(5-dimethylamino-naphthalene-1-sulfonyloxy)-1,2,3,4-tetrahydro-isoquinoline-3-carboxylic acid (1R): Compound **1R** (56%) was prepared as a pale yellow solid from **3A** (0.1 g, 0.52 mmol) and dansyl sulfonyl chloride (0.42 g; 1.56 mmol) as described for the synthesis of **5A**. M.p. 150–155 °C; ^{1}H NMR ([D$_6$]acetone, 400 MHz): δ = 8.67 (dd, J = 8.6, 1.0 Hz, 3-H), 8.50 (dd, J = 8.6, 1.2 Hz, 17-H), 8.38 (dd, J = 8.6 Hz, 6-H), 8.33 (dd, J = 7.8, 1.2 Hz, 15-H), 8.31 (d, J = 8.4 Hz, 20-H), 8.06 (dd, J = 7.3, 1.2 Hz, 1-H), 7.74 (dt, J = 8.0, 8.6, 1.0 Hz, 5-H), 7.60 (t, J = 7.6 Hz, 16-H), 7.52–7.59 (m, 2H, 2-H, 19-H), 7.37 (dd, J = 7.5, 0.8 Hz, 4-H), 7.20 (dd, J = 7.6, 0.8 Hz, 18-H), 7.09 (d, J = 8.3 Hz, 10-H), 6.74 (d, J = 2.4 Hz, 11-H), 6.59 (dd, J = 8.4, 2.5 Hz, 9-H), 5.00 (dd, J = 6.8, 2.0 Hz, 13-H), 4.63 (d, J = 16.4 Hz, 14-H$_a$), 4.50 (d, J = 16.4 Hz, 14-H$_b$), 3.23 (dd, J = 16.4, 2.0 Hz, 12-H$_a$), 3.01 (dd, J = 16.4, 6.8 Hz, 12-H$_b$), 2.92 (s, 6H, 7-H, 8-H), 2.86 ppm (s, 6H, 21-H, 22-H); elemental analysis calcd (%) for $C_{34}H_{33}N_3O_7S_2$: C 61.89, H 5.04, N 6.37; found: C 62.06, H 4.94, N 6.25. For more details about chemical characterization please refer to the Supporting Information.

3-(*S*)-2-(5-Dimethylamino-naphthalene-1-sulfonyl)-7-(5-dimethylamino-naphthalene-1-sulfonyloxy)-6,8-diiodo-1,2,3,4-tetrahydro-isoquinoline-3-carboxylic acid (2R): Compound **2R** (71%) was prepared from **1A** (0.1 g, 0.23 mmol) and dansyl sulfonyl chloride (0.186 g, 0.69 mmol) as described for the synthesis of **5A**. ^{1}H NMR ([D$_6$]DMSO, 200 MHz): δ = 8.64 (d, 3-H), 8.52 (d, 15-H), 8.1–8.38 (m, 2H, 1-H, 6-H), 8.19 (d, J = 7.8 Hz, 13-H), 8.14 (d, J = 7.6 Hz, 16-H), 7.77 (s, 19-H), 7.56–7.74 (m, 2H, 2-H, 5-H), 7.67 (t, J = 7.6 Hz, 14-H), 7.59 (t, J = 7.6 Hz, 17-H), 7.33 (d, 4-H), 7.26 (d, J = 8.4 Hz, 18-H), 4.98 (d, 11-H), 4.29 (dd, 2H, 12-H$_{a,b}$), 3.03 (d, 10-H$_a$), 3.17 (d, 10-H$_b$), 2.88 (s, 6H, 7-H, 8-H), 2.84 ppm (s, 6H, 21-H, 22-H); elemental analysis calcd (%) for $C_{34}H_{31}I_2N_3O_7S_2$: C 44.80, H 3.43, N 4.61; found C 45.00, H 3.34, N 4.51.

3-(*S*)-7-(5-Dimethylamino-naphthalene-1-sulfonyloxy)-2-(4-nitro-benzenesulfonyl)-1,2,3,4-tetrahydro-isoquinoline-3-carboxylic acid (3R): Compound **3R** (64%) was prepared from compound **6A** (0.05 g, 0.118 mmol) and 4-nitrophenylsulfonyl chloride (0.039 g, 0.176 mmol) under the conditions used for the synthesis of compound **1R**. ^{1}H NMR ([D$_6$]DMSO, 200 MHz): δ = 8.68 (d, J = 8.4 Hz, 3-H), 8.34 (2xd, J = 8.2 Hz, 2H, 15-H, 16-H), 8.29 (d, J = 8.6 Hz, 6-H), 8.34 (d, J = 7.8 Hz, 1-H), 7.85 (t, J = 8.4 Hz, 5-H), 7.83 (2xd, J = 8.2 Hz, 2H, 17-H, 18-H), 7.72 (t, J = 8.0 Hz, 2-H), 7.44 (d, J = 8.0 Hz, 4-H), 7.19 (d, J = 8.2 Hz, 10-H), 6.77 (d, J = 2.2 Hz, 11-H), 6.70 (dd, J = 2.2, 8.2 Hz, 9-H), 5.00 (t, J = 7.0 Hz, 13-H), 3.94 (d, J = 16.2 Hz, 14-H$_a$), 4.71 (d, J = 16.2 Hz, 14-H$_b$), 3.00–3.25 (m, 2H, 12-H$_{a,b}$), 2.98 ppm (s, 6H, 7-H, 8-H); elemental analysis calcd (%) for $C_{28}H_{25}N_3O_9S_2$: C 54.98, H 4.12, N 6.87; found: C 55.09, H 4.08, N 6.78.

3-(*S*)-7-(5-Dimethylamino-naphthalene-1-sulfonyloxy)-2-(4-nitro-benzoyl)-1,2,3,4-tetrahydro-isoquinoline-3-carboxylic acid (4R): Compound **4R** (73%) was prepared from **6A** (0.05 g, 0.118 mmol) and 4-nitrobenzoyl chloride (0.030 g, 0.176 mmol) under the conditions used for the synthesis of **1R**. ^{1}H NMR ([D$_6$]DMSO, 200 MHz): δ = 8.71 (d, J = 8.6 Hz, 3-H), 8.49 (2xd, J = 8.8 Hz, 2H, 17-H, 18-H), 8.40 (d, J = 8.6 Hz, 6-H), 8.29 (d, J = 9.0 Hz, 1-H), 8.17 (2xd, J = 8.8 Hz, 2H, 15-H, 16-H), 7.91 (t, J = 8.6 Hz, 5-H), 7.72 (t, J = 8.8 Hz, 2-H), 7.58 (d, J = 7.8 Hz, 4-H), 7.16 (d, J = 8.2 Hz, 10-H), 7.09 (d, J = 2.4 Hz, 11-H), 6.65 (dd, J = 2.4, 8.2 Hz, 9-H), 4.96 (t, J = 7.0 Hz, 13-H), 4.71 (d, J = 16.4 Hz, 14-H$_a$), 4.43 (d, J = 16.4 Hz, 14-H$_b$), 3.00–3.25 (m, 2H, 12-H$_{a,b}$), 2.96 (s, 6H, 7-H, 8-H); elemental analysis calcd (%) for $C_{29}H_{25}N_3O_8S$: C 60.51, H 4.38, N 7.30; found: C 60.28, H 4.50, N 7.49.

3-(*S*)-7-(5-Dimethylamino-naphthalene-1-sulfonyloxy)-2-(2-nitro-4-trifluoromethyl-benzenesulfonyl)-1,2,3,4-tetrahydro-isoquinoline-3-carboxylic acid (5R): Compound **5R** (90%) was prepared from compound **6A** (0.05 g, 0.118 mmol) and 2-nitro-4-trifluoromethylbenzenesulfonyl chloride (0.051 g, 0.176 mmol) under the conditions used for the synthesis of **1R**. ^{1}H NMR ([D$_6$]DMSO, 200 MHz): δ = 8.70 (d, 3-H), 8.39 (d, 6-H), 8.24 (s, 17-H), 8.16 (d, J = 7.6 Hz, 15-H), 8.15 (d, 1-H), 8.07 (d, J = 7.6 Hz, 16-H), 7.83 (t, 5-H), 7.72 (t, 2-H), 7.47 (d, 4-H), 7.35 (d, 10-H), 7.01 (s, 11-H), 6.72 (d, 9-H), 4.96 (t, 13-H), 4.71 (d, 14-H$_a$), 4.57 (d, 14-H$_b$), 3.20 (dd, 2H, 12-H$_{a,b}$), 2.96 ppm (s, 6H, 7-H, 8-H); elemental analysis calcd (%) for $C_{29}H_{24}F_3N_3O_9S_2$: C 51.25, H 3.56, N 6.18; found: C 51.13, H 3.64, N 6.23.

3-(*S*)-7-(5-Dimethylamino-naphthalene-1-sulfonyloxy)-2-(7,7-dimethyl-2-oxo-bicyclo[2.2.1]hept-1-yl-methanesulfonyl)-1,2,3,4-tetrahydro-isoquinoline-3-carboxylic acid (6R): Compound **6R** (15%) was prepared from **6A** (0.05 g, 0.118 mmol) and (7,7-dimethyl-2-oxobicyclo[2.2.1]hept-1-yl)methanesulfonyl chloride (0.074 g, 0.295 mmol) under the conditions used for the synthesis of **1R**. ^{1}H NMR ([D$_6$]DMSO, 200 MHz): δ = 8.71 (d, 3-H), 8.37 (d, 6-H), 8.20 (d, 1-H), 7.88 (t, 5-H), 7.74 (t, 4-H), 7.47 (d, 4-H), 7.29 (d, 10-H), 7.03 (s, 11-H), 6.73 (d, 9-H), 4.96 (t, 13-H), 4.71 (d, 14-H$_a$), 4.53 (d, 14-H$_b$), 3.61 (s, 2H, 15-H), 3.14 (dd, 2H, 12-H$_{a,b}$), 2.96 (s, 6H, 7-H, 8-H), 2.01–2.05 (m, 2H, 16-H), 1.95–2.00 (m, 1H, 17-H), 1.68–1.74 (m, 2H, 19-H), 1.40 (m, 2H, 18-H), 1.15 ppm (2s, 6H, 20-H, 21-H); elemental analysis calcd (%) for $C_{32}H_{36}N_2O_8S_2$: C 59.98, H 5.66, N 4.37; found: C 60.13, H 5.56, N 4.32.

3-(*S*)-7-(5-Dimethylamino-naphthalene-1-sulfonyloxy)-2-(naphthalene-2-carbonyl)-1,2,3,4-tetrahydro-isoquinoline-3-carboxylic acid (7R): Compound **7R** (80%) was prepared from **6A** (0.048 g, 0.113 mmol) and naphthalene-2-carbonyl chloride (0.032 g, 0.226 mmol) under the conditions used for the synthesis of **1R**. ^{1}H NMR ([D$_6$]DMSO, 200 MHz): δ = 8.70 (d, 3-H), 8.25 (d, 6-H), 8.05–8.12 (m, 4H, 16-H, 17-H, 20-H, 21-H), 8.07 (d, 1-H), 7.9 (d, 15-H), 7.85 (t, 5-H), 7.72 (t, 2-H), 7.68–7.77 (m, 2H, 18-H, 19-H), 7.49 (d, 4-H), 7.20 (d, 10-H), 6.91 (s, 11-H), 6.59 (d, 9-H), 4.10 (d, 14-H$_b$), 4.20 (dd, 14-H$_a$), 4.16 (dd, 14-H$_b$), 3.20 (dd, 2H, 12-H$_{a,b}$), 2.96 (s, 6H, 7-H, 8-H); elemental analysis calcd (%) for $C_{33}H_{28}N_2O_6S$: C 68.26, H 4.86, N 4.82; found: C 68.42, H 4.75, N 4.76.

3-(*S*)-7-(5-Dimethylamino-naphthalene-1-sulfonyloxy)-2-phenylmethanesulfonyl-1,2,3,4-tetrahydro-isoquinoline-3-carboxylic acid (8R): Compound **8R** (53%) was prepared from **6A** (0.050 g, 0.118 mmol) and phenylmethanesulfonyl chloride (0.032 g, 0.176 mmol) under the conditions used for the synthesis of **1R**. ^{1}H NMR ([D$_6$]DMSO, 200 MHz): δ = 8.70 (d, 3-H), 8.30 (d, 6-H), 8.20 (d, 1-H), 7.90 (t, 5-H), 7.80 (t, 2-H), 7.3–7.5 (m, 3H, 17-H, 18-H, 19-H), 7.30 (d, 4-H), 7.23 (d, 2H, 16-H, 20-H), 7.10 (d, 10-H), 6.90 (s, 11-H), 6.60 (d, 9-H), 4.90 (t, 13-H), 4.50 (dd, 14-H$_a$), 4.17 (dd, 14-H$_b$), 3.52 (s, 2H, 15-H), 3.15 (dd, 2H, 12-H$_{a,b}$), 2.96 (s, 6H, 7-H, 8-H); elemental analysis calcd (%) for $C_{29}H_{28}N_2O_7S_2$: C 59.98, H 4.86, N 4.82; found: C 59.75, H 4.97, N 4.94.

3-(*S*)-2-(4,5-Dibromo-thiophene-2-sulfonyl)-7-(5-dimethylamino-naphthalene-1-sulfonyloxy)-1,2,3,4-tetrahydro-isoquinoline-3-carboxylic acid (9R): Compound **9R** (69%) was prepared from **6A** (0.058 g, 0.137 mmol) and 4,5-dibromothiophene-2-sulfonyl chloride (0.070 g, 0.2 mmol) under the conditions used for the synthesis of **1R**. ^{1}H NMR ([D$_6$]DMSO, 200 MHz): $\delta = 8.70$ (d, 3-H), 8.40 (d, 6-H), 8.15 (d, 1-H), 7.85 (t, 5-H), 7.72 (t, 2-H), 7.49 (d, 4-H), 7.28 (d, 10-H), 7.13 (2xs, 2H, 11-H, 15-H), 6.78 (s, 9-H), 4.53 (t, 13-H), 4.25 (dd, 14-H$_a$), 4.16 (dd, 14-H$_b$), 3.20 (dd, 2H, 12-H$_{a,b}$), 2.96 (s, 6H, 7-H, 8-H); elemental analysis calcd (%) for $C_{26}H_{22}Br_2N_2O_7S_3$: C 42.75, H 3.04, N 3.84; found: C 42.97, H 2.92, N 3.73.

NMR spectroscopy: All NMR measurements were performed on a Bruker AMX 400 WB spectrometer operating at 9.395 Tesla (Centro Interdipartimentale Grandi Strumenti; University of Modena and Reggio Emilia) and equipped with a ^{1}H/BB probe head (NMR-tube diameter: 5 mm) optimized for inverse detection. Spectra were recorded for compound **1R** dissolved in [D$_6$]acetone. Compound **1R** was characterized fully on the basis of one-dimensional ^{1}H and {^{1}H}^{13}C NMR spectra and two-dimensional COSY, NOESY, and ^{1}H,^{13}C heterocorrelation (HETCOR) spectra.

Two-dimensional COSY spectra were recorded by using the following parameters: 2048 time-domain points (F_2 dimension) and 512 increments (F_1 dimension), spectral width: 4000 Hz, relaxation delay: 1 s, 8 transients per increment. Data were doubled in the F_1 dimension by zero filling and weighted by the sine-bell function in both dimensions prior to fast Fourier transform (FFT) in the magnitude mode.[23]

Two-dimensional 2D NOESY spectra were recorded with the following parameters: 2048 time-domain points (F_2 dimension) and 512 increments (F_1 dimension), spectral width: 4000 Hz, relaxation delay: 1 s, 8 transients per increment, mixing times: 25–500 ms. Data were doubled in the F_1 dimension by zero filling and weighted by the sine-square-bell function in both dimensions prior to FFT in the phase-sensitivity mode. Once NOEs had been detected, the data were reprocessed by using sine-square-bell and sine-bell window functions in the F_2 and F_1 dimensions, respectively, and by magnitude-mode calculation in the F_1 dimension to quantify the volume of the cross-peaks and avoid phase-twisting effects. In this way, the cross-peaks resulted exclusively in absorption mode, and a very good lineshape was maintained.[24–25]

Two-dimensional ^{1}H,^{13}C HETCOR spectra were recorded by using HMQC and HMBC pulse sequences to detect direct ($^1J_{CH}$) and long-range ($^nJ_{CH}$) proton–carbon correlations, respectively.[26–27] HMQC spectra were acquired by using the following parameters: 2024×256 data points, spectral width: 4000 Hz in the F_2 dimension, 10000 Hz in the F_1 dimension, recycle delay: 1 s, 32 scans, no ^{13}C decoupling. The evolution delay was fixed by considering an average value of 145 Hz for $^1J_{CH}$. FFT was performed by enhancement multiplication (line broadening: 1 Hz) in the F_2 dimension and by applying a sine-square-bell multiplication in the F_1 dimension (^{13}C). The same parameters were used for HMBC spectra, but with a larger spectral width in the ^{13}C dimension of 15000 Hz, an evolution delay corresponding to an average value of 7 Hz for $^nJ_{CH}$, and the application of a sine-square-bell function in the F_2 and F_1 dimensions prior to FFT.

Dihedral-angle determination: The dihedral angles were evaluated by processing the values of $^3J_{H,H}$ by using a modified Karplus equation. The translation of coupling constants into dihedral angles was based on the widely used empirical Karplus relationship, which is usually given by the formula $^3J = A + B\cos\Phi + C\cos 2\Phi$.[28] The coefficients depend both on the nature of the coupled nuclei and on the local chemical environment. Several attempts have been made by theoretical and experimental methods to refine Karplus coefficients for the different types of *J* coupling; however, the translation of ^3J coupling into dihedral angles is complicated by the intrinsic degeneracy of the Karplus relationship.[29]

Interatomic-distance determination: In all 2D NOESY spectra in the present study, only negative NOEs were detected. This observation raises the possibility of spin diffusion, which is taken into account by the term of indirect contribution in the equation that links NOE enhancement to interatomic distances.[30] For this reason, we considered the curves for the buildup of NOE enhancement, and the NOE enhancements used to derive the interatomic distances were taken at longer mixing times, when curves are again linear, that is, at an early stage of NOE buildup. In this way, an "initial rate approximation" was used, and the enhancements were considered proportional to $1/r^6$ (r indicates interatomic distance).[30] Moreover, the signal-to-noise ratios of the cross-peaks were high enough to allow precise measurement of the volumes of the cross-peaks. Because the molecular fragments considered are rather rigid, effects due to internal motion were neglected. By this procedure, we estimated interatomic distances. The three-dimensional conformation of compound **1R** was derived from the interatomic distances and dihedral angles, and the results were compared with data obtained by molecular modeling.

Molecular modeling: On the basis of the NMR spectroscopic data, a three-dimensional model of unbound **1R** was constructed by using the ChemOffice suite of programs.[31] The *O*-dansyl moiety was modeled on the basis of X-ray crystallographic data (1JG0), as NMR spectroscopy did not give suitable information about this part of the molecule.[14,32] A model of the three-dimensional ternary complex EcTS–dUMP–**1R** was constructed by using the 1JG0 X-ray crystal structure of the EcTS protein and the dUMP molecule. The model was subjected to energy minimization (Sander/AMBER 8.0) to relieve any unfavorable contacts.[33] Antechamber/AMBER 8.0 was used to prepare the **1R** molecule files needed for the minimization. All protein residues within 10 Å of the inhibitor and the ligand molecule were energy minimized with 20000 cycles of minimization (2000 cycles of steepest descendent plus 18000 cycles of conjugate gradient). The nonbonded cutoff distance was set at 10 Å. The conformational energies of the bound and unbound structures of compound **1R** were calculated with the AM1/SM2 Hamiltonian within AMSOL 6.6, whereby all bond lengths were left to be optimized but angles and dihedral angles were frozen.[34] Conformational analysis was performed on the torsions N–SO_2 and SO_2–R. A total of 1296 conformers were generated by incrementing each torsion by 10° at a time. The conformational energies were calculated with the AM1/SM2 Hamiltonian within AMSOL 6.6 by using the 1SCF keyword.

Biological activity: LcTS and EcTS were purified as described previously.[35–36] Enzyme kinetics experiments were conducted under standard conditions.[35–38] All compounds were screened for inhibitory activity against LcTS and EcTS. The inhibition experiments were conducted by measuring the effects of the inhibitor at different concentrations on the initial velocity of the enzyme in the presence of a limited amount of the folate substrate. IC_{50} values were determined, and apparent inhibition constants (K_i) were calculated as reported by assuming competitive inhibition for all compounds with respect to MTHF.[38]

Reactions were initiated by the addition of the enzyme. Stock solutions of each of the inhibitors were prepared freshly in dimethylsulfoxide (DMSO). The aqueous solubilities of the compounds were

determined by spectrophotometry. DMSO never exceeded a concentration of 5% in the reaction mixture. Each experiment was repeated at least three times, and no individual measurement differed by more than 20% from the mean. For low-activity binders, and to allow the analysis of structure–activity relationships throughout the series, the K_i value was calculated by assuming 2% inhibition at the solubility limit.

Acknowledgements

This research was supported by grants PRIN 2004/030405_004 and 2006/030430_004 (M.P.C.). We thank the CIGS (Centro Interdipartimentale Grandi Strumenti) and CICAIA (Centro Interdipartimentale di Calcolo Elettronico) of the University of Modena and Reggio Emilia for the use of instruments and computing facilities. We thank Dr. Rosaria Luciani for help in enzymatic testing, Dr. Federica Morandi, and Prof. Marcella Rinaldi for critical reading of the manuscript.

Keywords: enzyme inhibition · molecular recognition · NMR spectroscopy · species specificity · thymidylate synthase

[1] B. Hong, M. Haddad, F. Maley, J. H. Jensen, A. Kohen, *J. Am. Chem. Soc.* **2006**, *128*, 5636–5637.
[2] A. Gangjee, H. D. Jain, S. Kurup, *Anticancer Agents Med. Chem.* **2007**, *7*, 524–542.
[3] C. W. Carreras, D. V. Santi, *Annu. Rev. Biochem.* **1995**, *64*, 721–762.
[4] P. Bruni, G. Minopoli, T. Brancaccio, M. Napolitano, R. Faraonio, N. Zambrano, U. Hansen, T. Russo, *J. Biol. Chem.* **2002**, *277*, 35481–35488.
[5] A. Chernyshev, T. Fleischmann, A. Kohen, *Appl. Microbiol. Biotechnol.* **2007**, *74*, 282–289.
[6] D. Tondi, A. Venturelli, S. Ferrari, S. Ghelli, M. P. Costi, *J. Med. Chem.* **2005**, *48*, 913–916.
[7] M. P. Costi, S. Ferrari, A. Venturelli, S. Calo, D. Tondi, D. Barlocco, *Curr. Med. Chem.* **2005**, *12*, 2241–2258.
[8] L. W. Hardy, J. S. Finer-Moore, W. R. Montfort, M. O. Jones, D. V. Santi, *Science* **1987**, *235*, 448–455.
[9] M. P. Costi, *Med. Res. Rev.* **1998**, *18*, 21–42.
[10] D. Tondi, U. Slomczynska, M. P. Costi, D. M. Watterson, S. Ghelli, B. K. Shoichet, *Chem. Biol.* **1999**, *6*, 319–331.
[11] S. P. Miller, M. Lunzer, A. M. Dean, *Science* **2006**, *314*, 458–461.
[12] A. L. van Bueren, A. B. Boraston, *J. Mol. Biol.* **2007**, *365*, 555–560.
[13] M. Glasner, J. Gerlt, P. Babbitt, *Adv. Enzymol. Relat. Areas Mol. Biol.* **2007**, *75*, 193–239.
[14] T. A. Fritz, D. Tondi, J. S. Finer-Moore, M. P. Costi, R. M. Stroud, *Chem. Biol.* **2001**, *8*, 981–995.
[15] M. Lang, S. De Pol, C. Baldauf, H.-J. Hofmann, O. Reiser, A. G. Beck-Sickinger, *J. Med. Chem.* **2006**, *49*, 616–624.
[16] T. Ganesh, R. C. Guza, S. Bane, R. Ravindra, N. Shanker, A. S. Lakdawala, J. P. Snyder, D. G. I. Kingston, *Proc. Natl. Acad. Sci. USA* **2004**, *101*, 10006–10011.
[17] S. E. Gibson, N. Guillo, J. O. Jones, I. M. Buck, S. B. Kalindjian, S. Roberts, M. J. Tozer, *Eur. J. Med. Chem.* **2002**, *37*, 379–389.
[18] E. Kellenberger, G. Mer, C. Kellenberger, G. Marguerie, J. F. Lefèvre, *Eur. J. Biochem.* **1999**, *260*, 810–817.
[19] S. Wielert-Badt, J. T. Lin, M. Lorenz, S. Fritz, R. K. H. Kinne, *J. Med. Chem.* **2000**, *43*, 1692–1698.
[20] N. C. Gonnella, R. Bohacek, X. Zhang, I. Kolossvary, C. G. Paris, R. Melton, C. Winter, S. Hu, V. Ganu, *Proc. Natl. Acad. Sci. USA* **1995**, *92*, 462–466.
[21] C. A. Hunter, J. K. M. Sanders, *J. Am. Chem. Soc.* **1990**, *112*, 5525–5534.
[22] K. Verschueren, *Synthesis* **1992**, 458–461.
[23] W. P. Aue, E. Bartholdi, R. R. Ernst, *J. Chem. Phys.* **1976**, *64*, 2229–2246.
[24] J. Jeener, B. H. Meier, P. Bachmann, R. R. Ernst, *J. Chem. Phys.* **1979**, *71*, 4546–4553.
[25] A. G. Redfield, S. D. Kunz, *J. Magn. Reson.* **1975**, *19*, 250–254.
[26] A. Bax, M. F. Summers, *J. Am. Chem. Soc.* **1986**, *108*, 2093–2094.
[27] R. H. Griffey, C. D. Poulter, A. Bax, B. L. Hawkins, Z. Yamaizumi, S. Nishimura, *Proc. Natl. Acad. Sci. USA* **1983**, *80*, 5895–5897.
[28] M. Karplus, *J. Am. Chem. Soc.* **1963**, *85*, 2870–2871.
[29] C. A. Haasnoot, F. A. de Leeuw, C. Altona, *Tetrahedron* **1980**, *36*, 2783–2792.
[30] Y. Lin, B. Rao, D. Nageswara, *Biochemistry* **2000**, *39*, 3636–3646.
[31] CambridgeSoft Corporation.
[32] H. M. Berman, J. Westbrook, Z. Feng, G. Gilliland, T. N. Bhat, H. Weissig, I. N. Shindyalov, P. E. Bourne, *Nucleic Acids Res* **2000**, *28*, 235–242.
[33] D. A. Case, T. A. Darden, T. E. Cheatham, C. L. Simmerling, J. Wang, R. E. Duke, R. Luo, K. M. Merz, B. Wang, D. A. Pearlman, M. Crowley, S. Brozell, V. Tsui, H. Gohlke, J. Mongan, A. Kollman, AMBER 8, University of California, San Francisco, **2004**.
[34] G. D. G. Hawkins, G. C. Lynch, C. C. Chambers, I. Rossi, J. W. Storer, J. Li, P. Winget, D. Rinaldi, D. A. Liotard, C. J. Cramer, D. G. Truhlar, AMSOL version 6.6, University of Minnesota, Minneapolis, **1997**.
[35] S. Climie, D. V. Santi, *Proc. Natl. Acad. Sci. USA* **1990**, *87*, 633–637.
[36] V. J. Davisson, W. Santi, D. V. Sirawaraporn, *J. Biol. Chem.* **1989**, *264*, 9145–9148.
[37] V. J. Davisson, W. Sirawaraporn, D. V. Santi, *J. Biol. Chem.* **1994**, *269*, 30740.
[38] I. H. Segel, *Enzyme Kinetics: Behavior and Analysis of Rapid Equilibrium and Steady-State Enzyme Systems*, Wiley-Interscience, New York, **1975**, p. 105.

Received: September 4, 2007

